SAND2017-13482J

# A Simplified Quantitative Model for Fissile Material Production from Fast Spallation Neutrons

David R. Farley
Sandia National Laboratories*

7011 East Avenue, Livermore, California 94550

Abstract

The Accelerator Driven System (ADS) as a reactor to produce fissile material, or for partitioning & transmutation purposes, has potential as an inherently safe reactor since it can be shut down by simply turning off the accelerator. Multiple studies have focused on the intranuclear and internuclear physics involved in the spallation process for high-energy projectiles impacting high-Z targets relevant to ADS applications. To quantify spallation neutronics, and thereby fissile material production, generally requires numerical methods such as MCNP, and such calculations are specific to the geometry under consideration. This study uses published cross sections from the ENDF database and an assumed generic cylindrical geometry for the ADS target and fertile blanket to derive analytic expressions for the production of Pu-239 and U-233, without needing to run MCNP codes, yet matching published data.

## Introduction

Much research has been done on understanding spallation neutron generation [1], [2], [3], [4] with application to Accelerator Driven Systems (ADS) [5]. These studies can roughly be divided into thin target [6], [7], [8], [9], [10], [11], [12] and thick target [13], [14], [15], [16], [17], [18] theories and experiments. Thin target research focuses on understanding *intranuclear* physics, whereas thick target research accounts for secondary *internuclear* reactions that can occur due to the extended length or diameters of such thick targets. While some studies have involved heavier impacting projectiles than protons/deuterons, this study will remain concentrated on just these lighter hydrogen projectiles. Further, although there is some minor benefit in using deuterons over protons for spallation neutron production, the difference is not significant [2], so protons will be assumed as the impacting projectiles herein. Also, we will assume the ADS target to be lead or uranium (natural or depleted), and a uranium breeder blanket. An illustration of a

* Sandia National Laboratories is a multimission laboratory managed and operated by National Technology and Engineering Solutions of Sandia LLC, a wholly owned subsidiary of Honeywell International Inc. for the U.S. Department of Energy's National Nuclear Security Administration under contract DE-NA0003525.

simplified ADS system is shown in Fig. 1. Note that a moderator is not shown in Fig. 1, but could be envisioned as an annulus between the Pb or U ADS target and the U blanket.

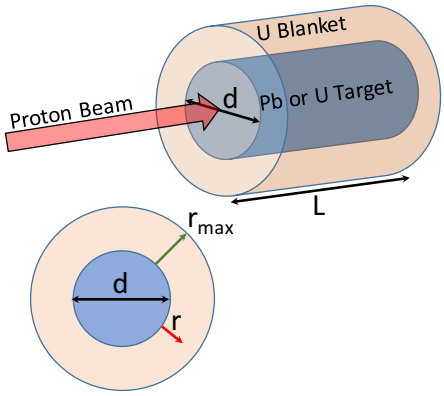


**Figure 1**. Illustration of a simplified ADS system, assuming a Pb or U target struck by high-energy protons, surrounded by a uranium breeder blanket. While no moderator is shown here, one could be inserted as an annulus between the ADS target and U blanket to slow the spallation neutrons towards a thermal spectrum. The diameter of the ADS target is $d$, with a length $L$, and the radial distance from the ADS target surface is $r$.

## Thin Targets

Although the main focus of this study will be on thick target approximations, it is worthwhile to briefly provide some background on thin target results. In general, the thin target models involve an intranuclear cascade (INC) stage followed by an evaporation stage [6], and although refinements to this model have been made [13], the average number of spallation neutrons produced *per reaction* (neutron multiplicity $M_n$) in a thin target can be approximated by [6]

$$M_n = (0.0803 + 0.0336 \ln E_p) A_t \qquad (1)$$

where $E_p$ is the proton energy in GeV and $A_t$ is the target atomic mass. Note that *per reaction* is a more important distinction when considering thick targets, for in thin targets just one reaction occurs (with low probability) whereas in thick targets multiple reactions are possible throughout the extent of the target. A plot of spallation neutron multiplicity versus impacting proton energy for lead and uranium targets using Eq. (1) is shown in Fig. 2. Hereafter, one could consider these values the minimum possible for these target materials, and as will be shown much larger multiplicities are possible for thick targets due to multiple reactions occurring (both primary and secondary particle interactions).

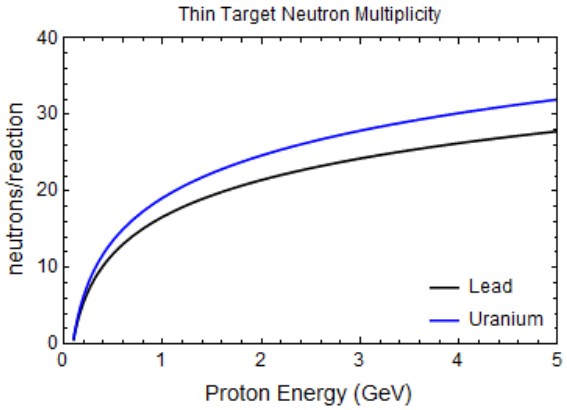

**Figure 2**. Neutron multiplicity versus impacting proton energy for thin lead and uranium targets, per Eq. (1) of Cugnon [6].

## Thick Targets

With thick targets, consideration must be made for the survival probability of the impacting protons, given as $1\text{-}P_r = \exp(\text{-}L/L_{int})$ where $P_r$ is the reaction probability, $L$ is the length along the target, and $L_{int}$ is the characteristic interaction length. For lead targets, $L_{int}$ = 18.4 cm [4], and for uranium $L_{int}$ = 11.4 cm [2]. The proton survival probabilities for lead and uranium targets are shown in Fig. 3. As shown, it is very likely a proton has reacted prior to the end of long targets of the order 60 cm for uranium and 100 cm for lead, and therefore not much reason for targets longer than these.

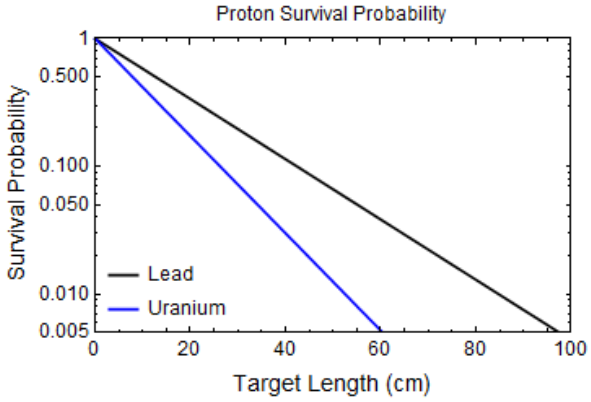


**Figure 3.** Survival probability of impacting protons striking lead and uranium targets.

To convert neutron multiplicity per reaction into neutron yield $Y_n$ per incoming proton, one must multiply the reaction probability $P_r$ with $M_n$. For thin targets, the reaction probability is low, but constant, whereas for thick targets there is a larger chance of interaction.

### Magill & Peerani Simple Neutron Yield Model

Per Magill & Peerani [19], for a cylindrical target 10 cm in diameter and 60 cm in length, the neutron yield is given by

$$Y_n = c_m(E_p - 0.12\ \text{GeV}) \qquad \text{for } E_p > 0.12\ \text{GeV} \tag{2}$$

where $c_m$ is a coefficient that is 22.7 for lead (Pb) and 36.7 for depleted uranium (U-238) targets which are 10 cm in diameter and 60 cm length [20]. However, while this simple model is appealing, it was calculated for a particular target and does not necessarily provide confidence that this model is applicable to arbitrary target dimensions and proton energies. Therefore, a more comprehensive investigation is done below, applicable to arbitrary target size and proton energy, in a simple analytic solution without needing to run Monte Carlo codes for each specific case.

## Background on Thick Target Models

A number of different thick target experiments and modeling have been conducted by several groups, as illustrated in Fig. 4. As seen in Fig. 4, the thick 20 cm diameter, 60 cm length lead targets of Nikolaev/Vassil'kov [14], [15] and the high proton energy data (12 GeV) of Arai [17] are fit well by all three models of Bauer [1], Yurevich [13], and Arai [17]. However, these models overestimate the neutron yield for not as large of targets, such as the data of Fraser [18] with a 10 cm diameter by 61 cm length Pb target, as well as data from Pienkowski [4] and Letourneau [3] with 15 cm diameter by 35 cm length Pb targets. For uranium targets, Hilscher [2] states that multiplying lead target neutron yields by 1.46 adequately represents uranium. The model of Carpenter of neutron yield ($-6 + 50E_p$) for uranium targets is a purely linear fit through a small number of data points that do not exceed 1.5 GeV proton energy. Since the data of Hilscher is more complete and shows a nonlinear fit at higher proton energies, the model of Hilscher will be assumed here to be more valid. Additionally, it is not clear whether Carpenter or Hilscher are correctly plotting Fraser's data [18] in their published figures.

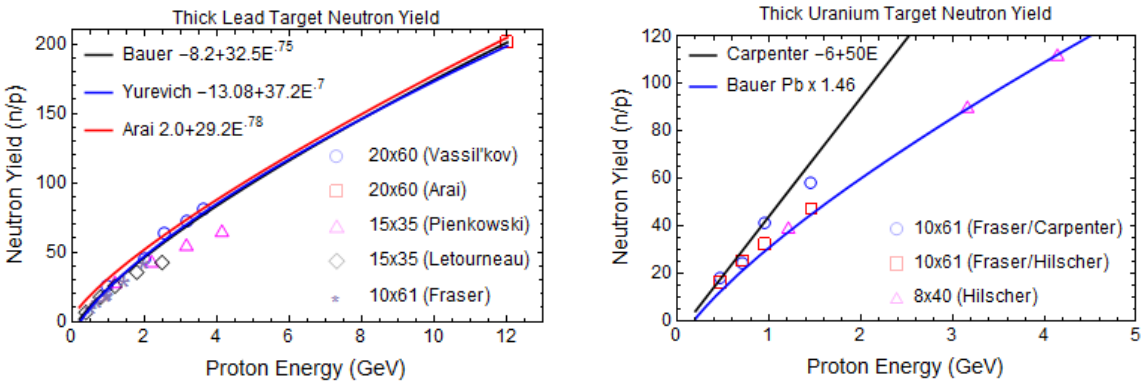


(a) (b)

**Figure 4.** (a) Thick Pb target neutron yield (spallation neutrons per incoming proton) experimental data from a number of research groups and associated models; and (b) models for both uranium and lead thick targets.

Assuming that any practical ADS target design will maximize its length to achieve maximal reaction probability, the radial dimension drives the amount of spallation neutrons that escape the target. These escaping spallation neutrons can then be used for other purposes such as minor actinide transmutation or fissile material production. For Pb targets, the radial dependence of neutron escape was calculated by Hashemi-Nezhad [5], which is reproduced in Fig. 5(a). From this data, a best fit is parameterized here as

$$Y_{n_{\mathrm{Pb}}}(d) = 30\left(1 - 0.6e^{-d/20\mathrm{cm}}\right) \qquad (3)$$

The applicable experimental data given in Letourneau *et al* [3] is also shown in Fig. 5(a) for a 25 cm long Pb target, normalized to 1 GeV impacting proton energy.

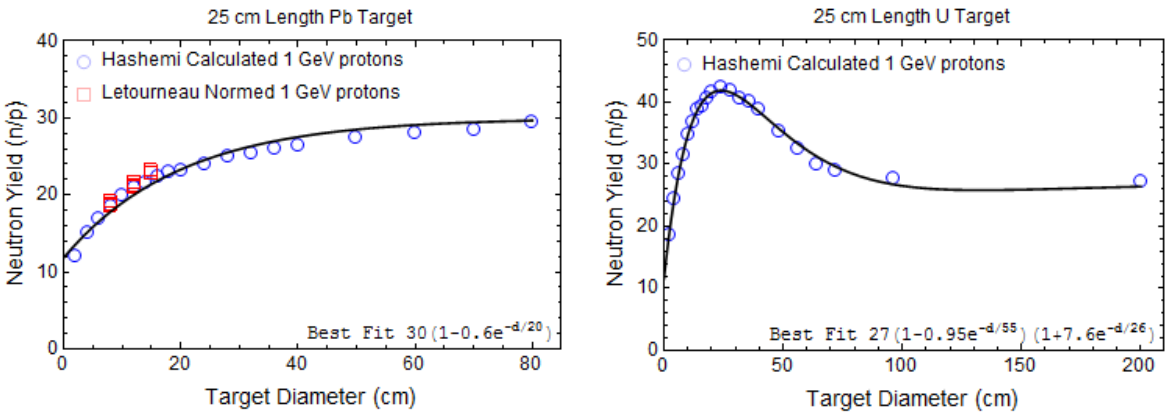


(a) (b)

**Figure 5.** Calculated dependence of neutron escape from a lead target based on the results of Hashemi-Nezhad [5], including a best fit parameterization as a function of target diameter, for (a) 25 cm long Pb target along with normalized experimental data of Letourneau [3]; and (b) 25 cm long uranium target.

For uranium targets, the dependence of escaping neutrons on radial direction is more complicated due to the greatly enhanced possibility of neutron absorption. Shown in Fig. 5(b) is the radial dependence of neutron yield for a 25 cm long uranium target, again as calculated by Hashemi-Nezhad [5]. No experimental data could be found in the literature for neutron escape as a function of target diameter. The fit for this dependence is found here to be best approximated as

$$Y_{n_U}(d) = 27\left(1 - 0.95e^{-d/55\text{cm}}\right)\left(1 + 7.6e^{-d/26\text{cm}}\right) \quad (4)$$

Thus, using the proton reaction probability 1- exp(-$L/L_{int}$), as can be inferred from Fig. 3, along with the fits estimated through Eqs. (3) and (4), one now has a means to easily calculate neutron yield (escaping from the target) for Pb and U targets, respectively. Note that for uranium one would expect a nonlinear escape profile along the axial direction, analogous to the radial escape profile of Fig. 5(b). However, the length of the target is used to maximize the probability of a proton reaction (Fig. 3) which is naturally co-linear with the direction of the incoming protons (i.e. axial), whereas the diameter of the target should be optimized for maximum escape probability (if the intent is to use as many spallation neutrons as possible for a subsequent process such as transmutation or fissile material production). One therefore can think of the target length and diameter to be of orthogonal intent – optimize length for full use of the incoming protons; optimize diameter for maximizing escaping spallation neutron flux.

## Generalization of thick target models for arbitrary length and diameters

Now that the form of the spallation neutrons fates as a function of length and diameter are characterized, a generalized framework is possible. The model of Bauer [1] will be used for thick lead targets, and Hilscher's [2] recommendation of simply multiplying Bauer's model by 1.46

for uranium, normalized by the 20x60 cm targets, are used to give the generalized neutron yield per proton equations as

$$Y_{n_{\mathrm{Pb}}}(E_p, L, d) = 1.33(-8.2 + 32.5E_p^{0.75})(1 - 0.6e^{-d/20})(1 - e^{-L/18.4}) \quad (5)$$

$$Y_{n_{\mathrm{U}}}(E_p, L, d) = 0.96(-8.2 + 32.5E_p^{0.75})(1 - 0.95e^{-d/55})(1 + 7.6e^{-d/26})(1 - e^{-L/11.4}) \quad (6)$$

Plots of Eqs. (5) and (6) are illustrated in Figs. 6 (a) and (b), respectively, along with relevant experimental data points. As shown in Fig. 6(a), the modeling now better follows the smaller Pb target sizes used by Fraser (10x61 cm) [18] as well as Letourneau [3] and Pienkowski [4] for their 15x35 cm Pb targets. Similarly, experimental data for uranium targets shown in Fig. 6(b) also illustrates how uranium target geometry affects the neutron yield. Note that the data of Arai [17] at 12 GeV is not shown in Fig. 6(a) to highlight the fit at lower energies, but the model does intersect the Arai yield of 201 n/p at 12 GeV. Also note that the uranium experimental results of Fraser [18] as reported Carpenter [16] appear to follow a 20x60 target dimension, whereas Fraser states his target was 10x60. Fraser's data as reported by Hilscher does appear to follow our current model, though the data spread is sufficient such that a variety of target sizes could also adequately fit the data. However, since the other uranium data of Hilscher [2] does follow our model, and Fraser's data (as reported by Hilscher) also follows our model, we will assume that uranium target modeling has been adequately addressed.

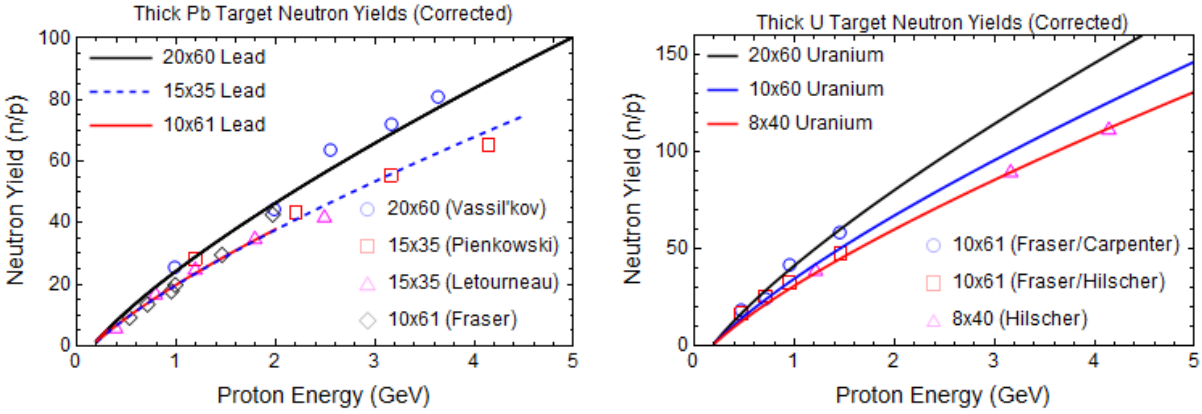


**Figure 6.** Models for thick target neutron yields, corrected for arbitrary target length and diameter, for (a) lead targets; and (b) uranium targets.

## Spallation Neutron Spectra

Findlay [21] provided a generalized 'back of the envelope' model for spallation neutron spectra, which appears to provide reasonable results (within a factor of 2) for a variety of target materials (Pb, U, W, Ta), noting that all spallation neutron spectra have a similar profile regardless of target or impacting proton energy (order of 1 GeV). The form of the generalized spectra as a function on neutron energy $E_n$ is given by Findlay as

$$f^{\text{spallation}}(E_n) = \begin{cases} \frac{1}{0.6} E_n^{-1/2} & 0.1 \text{ MeV} \le E_n \le 0.6 \text{ MeV} \\ E_n^{-3/2} & 0.6 \text{ MeV} \le E_n \le 100 \text{ MeV} \\ 100 E_n^{-5/2} & E_n \ge 100 \text{ MeV} \end{cases} \quad (7)$$

This relation is illustrated in Fig. 7 as Findlay > 0.1 MeV. Note that $f^{\text{spallation}}$ has not been normalized, though its integral regardless of upper energy limit is approximately 4. This model does not include neutron energies below 0.1 MeV, and the high energy limit of the neutron spectra should coincide with the impacting proton beam energy (though the yield at these energies is very low).

There certainly is a lower energy tail for spallation neutrons, and it is different for lead and uranium targets. By studying published results, we find that the neutron energy scales as $E_n^{1/2}$ for $E_n < 0.3$ MeV for lead targets [14], [15], [16], and as $E_n^{5/3}$ for $E_n < 0.1$ MeV for uranium targets [5], [16]. These tails are also shown in Fig. 7 as low-energy appendages to the nominal Findlay model.

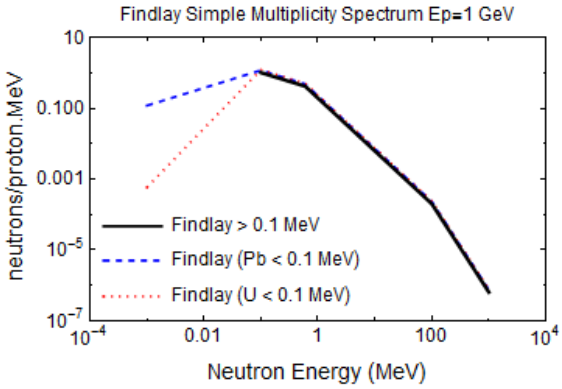


**Figure 7.** The generalized spallation neutron spectrum estimated by Findlay [21] along with our additions of the low energy tails separately for lead and uranium.

Note, however, that integration from the lower limit of the low-energy tails will now result in different normalization between lead and uranium targets. Also, upon examination of published spectra [5], [14], [15], [16], there are slight differences between lead and uranium target spectra at intermediate energies. Taking all of this into account, separate modified spectra models were derived as

$$f_{\text{Pb}}^{\text{spallation}}(E_n) = \begin{cases} \frac{1}{0.36} E_n^{1/2} & E_n \le 0.3 \text{ MeV} \\ \frac{1}{1.2} E_n^{-1/2} & 0.3 \text{ MeV} \le E_n \le 1.2 \text{ MeV} \\ E_n^{-3/2} & 1.2 \text{ MeV} \le E_n \le 100 \text{ MeV} \\ 100 E_n^{-5/2} & E_n \ge 100 \text{ MeV} \end{cases} \quad (8)$$

$$f_{\mathrm{U}}^{\text{spallation}}(E_n) = \begin{cases} 5100E_n^{5/3} & E_n \le 0.1\ \text{MeV} \\ 11E_n^{-1} & 0.1\ \text{MeV} \le E_n \le 0.9\ \text{MeV} \\ 10E_n^{-2} & 0.9\ \text{MeV} \le E_n \le 100\ \text{MeV} \\ 100E_n^{-5/2} & E_n \ge 100\ \text{MeV} \end{cases} \quad (9)$$

These spectra are shown in Fig. 8 (integral equals total neutron yield per proton for 15x30 cm targets). To obtain the actual quantitative spectra for a prescribed target type and size, the neutron yield estimates $Y_n(E_p, L, d)$ of Eqs. (5) & (6) are multiplied to these spectra, after being normalized.

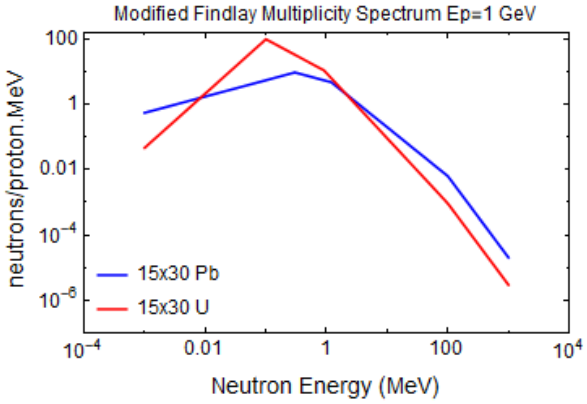


**Figure 8.** Normalized general spectra models for lead and uranium targets, following Eqs. (8) & (9), as well as the original generalized model of Findlay [21].

## Fission Neutron Production

The multiplicity of fission neutrons $\nu(E_n)$ as a function of incident neutron energy is given by Eqs. (10) & (11) for U-238 and U-235 targets, respectively [22]. These equations are plotted in Fig. 10.

$$\nu^{\text{U-238}}(E_n) = 2.41 + 10.24(1 - e^{-0.015E_n}) \quad (10)$$

$$\nu^{\text{U-235}}(E_n) = 2.31 + 9.33(1 - e^{-0.017E_n}) \quad (11)$$

Since we will only be interested in the dominant U-238 atoms of the uranium blanket (or assuming purely depleted uranium blanket), the multiplicity equation of Eq. (10) is integrated with respect to the spallation neutron spectra of Eqs. (8) & (9) for Pb and U ADS targets (see Fig. 9), which results in an average multiplicity of 3.39 for lead ADS targets and 2.62 for uranium ADS targets.

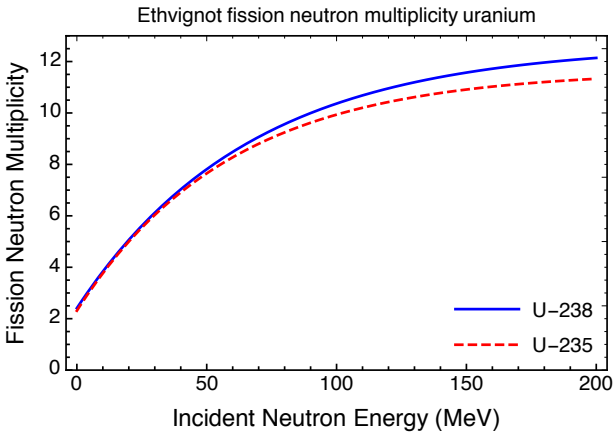


**Figure 9**. Fission neutron multiplicities for U-238 and U-235 as a function of incident neutron energy [22].

### Fission Neutron Spectra

The normalized fission neutron spectrum for uranium is accurately given by [23]

$$f_{\mathrm{U}}^{\mathrm{fission}}(E_n) = \sqrt{E_n} e^{-\frac{E_n}{1.29}} / 1.299 \qquad (12)$$

where $E_n$ is in MeV. Equation (12) is plotted in Fig. 10.

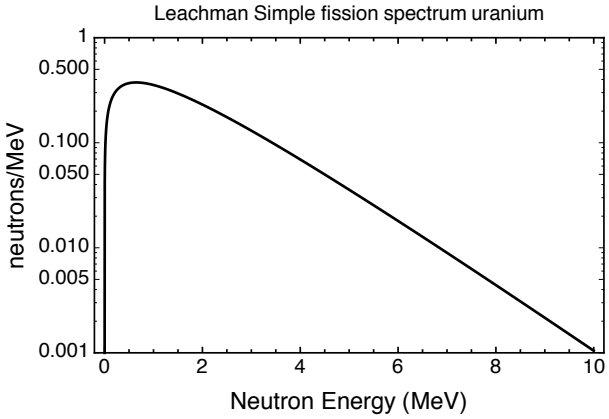


**Figure 10.** Prompt fission neutron spectrum from uranium (normalized to unit area) [23].

Thus, multiplying Eq. (12) by 3.39 or 2.62 for Pb or U ADS targets, respectively, we have the energy-dependent number of fission neutrons available within the uranium blanket.

## Plutonium Production

According to Magill & Peerani [19], the fissile atom production rate, in this case Pu-239 atoms, is simply given as

$$\dot{n}_{\text{Pu-239}} = \eta \, i_p Y_n \qquad \text{[atoms/sec]} \qquad (13)$$

where coefficient $\eta \approx 1 - 2$, as was estimated using the 1-D neutron transport code XSDRNPM module from the SCALE system [24]. Magill & Peerani used the linear neutron yield

formulation of Gilmore *et al* [20] when deriving a value for $\eta$ with Eq. (13), but we will assume Eq. (13) is applicable regardless of the specific formulation for $Y_n$. Again, this simple model of Magill & Peerani is based on a specific target calculation, generalized for broader use. Below we perform a more detailed investigation, yet still arriving at a relatively simple, analytic solution for plutonium production rate (or other actinide production, with the appropriate cross sections).

Having the neutron yields for spallation and fission, including their energy dependence, plutonium production rates can be calculated using interaction cross sections. The neutron interaction cross sections as tabulated in the Evaluated Nuclear Data File (ENDF) database (ENDF/B-VII.1) is used to calculate neutron-induced production and decay rates. The nuclear chain for creation of plutonium from uranium is shown in Fig. 11 [25]. While specifics are discussed in the figure caption, the primary channel for Pu-239 production is

$$^{238}\mathrm{U} \rightarrow {}^{239}\mathrm{U} \rightarrow {}^{239}\mathrm{Np} \rightarrow {}^{239}\mathrm{Pu} \qquad (14)$$

where U-239 is created through radiative neutron capture by U-238, and Np-239 and Pu-239 result from subsequent natural $\beta^-$ decays (23.45 mins and 2.356 days, respectively). The transmutation path of U-235 is not considered since it will be such a small mass fraction in a uranium blanket (0.7 wt% in natural uranium; much less in depleted uranium).

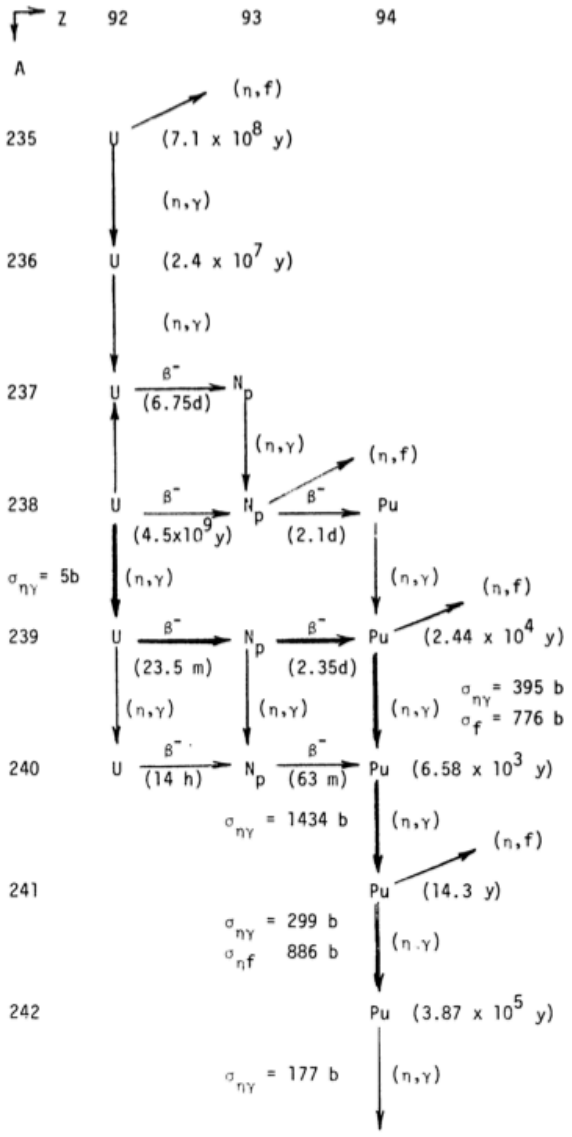


**Figure 11.** Plutonium production scheme from uranium [25]. U-239 is created through radiative neutron capture by a U-238 atom, where thereafter $\beta^-$ decays into Np-239 (half-life 23.5 mins). The Np-239 then $\beta$ decays to Pu-239 with a half-life of 2.35 days. The channels to produce Pu-239 through $\beta$ decay of U-238 is too slow to be significant (half-life 4.5 billion years); and production from U-237 is also ignored since U-237 has a very small mass fraction in natural uranium, and the two radiative capture reactions further reduce the probability that this channel could generate even minor amounts of Pu-239. Besides natural decay of isotopes, the neutron-induced transmutation of U-239, Np-239, and Pu-239 must also be considered since these reactions can significantly deplete the populations of these isotopes. Note that the cross sections depeicted are averages for a thermal neutron spectrum, as would be expected with a moderated fission reactor.

Cross sections for U-238, U-239, Np-239 and Pu-239 were downloaded from the ENDF/B-VII.1 library (http://www.nndc.bnl.gov/exfor/endf00.jsp) for neutron energies starting at 100 eV and extending to 20 or 30 MeV (as far as the data exists for these isotopes). This upper limit of 20-30 MeV is acceptable since the spallation neutrons are few at these higher energies by more than an order of magnitude compared to ~1 MeV neutron energies (see Fig. 8). The neutron reactions considered are radiative neutron capture $\sigma^{(n\gamma)}$, fission $\sigma^{(nf)}$, and the $\sigma^{(n,2n)}$ , $\sigma^{(n,3n)}$ , $\sigma^{(n,4n)}$ cross sections. To account for neutron-induced decay of the isotopes, all these cross section are added to calculate the absorption cross section $\sigma^{(abs)}$.

Radiative neutron capture by U-238 to create U-239, and thus start the chain towards Pu-239 production, are considered via two paths: (1) the initial passage of spallation neutrons from the ADS target source; and (2) a second wave of fission neutrons created by the initial wave of

spallation neutrons. The ordinary differential equations representative of these two waves of neutrons within the uranium blanket are described in the following sections.

## Spallation Neutron Flux

The number of incident protons per second, $i_p$, is the proton current (Amperes) divided by $1.6\text{x}10^{-19}$ C. From Fig. 1, we see that the area traversed by spallation neutrons escaping the ADS target surface is $2\pi L(d/2 + r)$. The survival probability of neutrons as a function of radius from the ADS target surface is $\exp(-n_{\text{U-238}}\sigma^{(\text{abs})}r)$. Thus, the spallation neutron flux is given by

$$\Phi^{\text{spallation}}\left(E_n, E_p, r, d, L\right) = \frac{i_p Y_n(E_p,d,L) f^{\text{spallation}}(E_n)}{2\pi L(\frac{d}{2}+r)} e^{-n_{U238}\sigma_{\text{U-238}}^{(\text{abs})}(E_n)r} \tag{15}$$

with units of [neutrons/cm$^2$.MeV.sec] and where $Y_n(E_p,d,L)$ is the spallation neutron yield per incident proton [see Eqs. (5) and (6)]. For clarity, the terms of Eq. (15) that depend on the spallation neutron energy $E_n$ can be separated from other terms, as

$$\Phi^{(s)}\left(E_n, E_p, r, d, L\right) = \phi_0^{(s)}(E_p, r, d, L) f^{(s)}(E_n) e^{-n_{\text{U-238}}\sigma_{\text{U-238}}^{(\text{abs})}(E_n)r} \tag{16}$$

where $\phi_0^{(s)}\left(E_p, r, d, L\right) = i_p Y_n(E_p, d, L)/2\pi L(d/2 + r)$ [neutrons/cm$^2$.sec], the normalized spallation neutron spectrum $f^{(s)}$ is in units of 1/MeV, and the superscript ($s$) represents "spallation". The differential reaction rate d$R$/d$E_n$ (cm$^3$/MeV.sec) is the neutron flux multiplied by the relevant reaction ($j$) cross section (abs, n$\gamma$, etc.) for the $i$th isotope:

$$\frac{dR_i^{(j)}(E_n,E_p,r,d,L)}{dE_n} = \Phi^{(s)}\left(E_n, E_p, r, d, L\right) \cdot \sigma_i^{(j)}(E_n) \tag{17}$$

Since U-238 is the dominant isotope and will be mainly constant for exposure times of interest, we will assume $n_{\text{U-238}}$ is a constant density throughout. As a first step, we will integrate over spallation neutron energy $E_n$, which essentially only involves the generic integral shown in Eq. 18(a) to give the energy-averaged, radially decaying flux, cross section as a function of radius $r$ from the ADS target surface as

$$\langle\sigma_i^{(j)}(r)\rangle = \int dE_n \cdot f^{(s)}(E_n) \exp\left[-n_{\text{U238}}\sigma_{\text{U-238}}^{(\text{abs})}(E_n)r\right] \cdot \sigma_i^{(j)}(E_n) \tag{18a}$$

such that

$$R_i^{(j)}\left(E_p, r, d, L\right) = \phi_0^{(s)}\left(E_p, r, d, L\right) \cdot \langle\sigma_i^{(j)}(r)\rangle \tag{18b}$$

Note that the form of the integral in Eq. (18a) will be the same in all cases considered here, with just the cross section term $\sigma_i^{(j)}$ varying per reaction.

The energy-averaged, radially decaying flux cross section $\langle\sigma(r)\rangle$ for all reactions were found to have the piecewise-continuous form $\langle\sigma_i^{(j)}(r)\rangle = \langle\sigma_i^{(j)}(r_0)\rangle\left[\alpha e^{-r/r_a} + (1-\alpha)e^{-r/r_b}\right]$. Therefore, all that is needed are the $\langle\sigma_i^{(j)}(r_0)\rangle$ cross sections evaluated at $r = r_0$, weighting term $\alpha$, and the attenuation lengths $r_a$ and $r_b$ for the reactions, which then greatly simplifies the

calculation of the reaction rates of Eq. (18b). As examples, the energy-averaged, radially decaying flux, cross sections for U-238 for both lead and uranium ADS targets are shown graphically as a function of radius $r$ from the ADS target surface in Figs. 12 (a) and (b), respectively. As can be seen from the figures, the fits (red lines) overlay the calculated points (blue disks) quite well. Similar good fits were obtained for all other cross section calculations. The collected cross section parameters for U-238, U-239, Np-239 and Pu-239 are given in Table 1. Note that while the (n,2n), (n,3n) and (n,4n) reactions are not listed in Table 1 for clarity, they were included in the total absorption cross sections $\sigma^{(abs)}$. There are three radial regions for the fits: $0 < r < r_0 = 100$ cm; 100 cm $< r < r_0 = 500$ cm; and $r > r_0 = 500$ cm. Breaking the overall fit parameters into three regions allowed for much more accurate piecewise-continuous fits rather than one fit for all $r$.

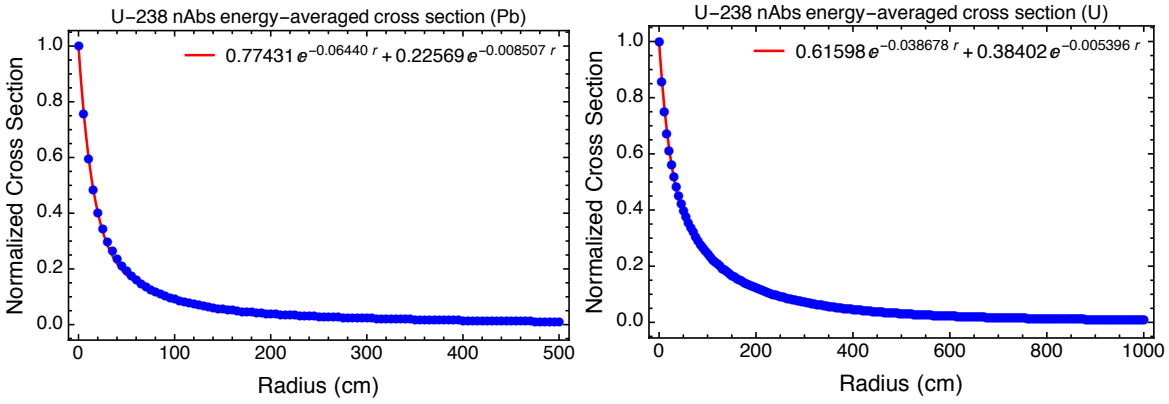


(a) (b)

**Figure 12.** The spallation energy-averaged neutron absorption cross section, including the exponential neutron flux decay through the uranium blanket, as a function of radius $r$ from the ADS target surface for (a) a lead ADS target; and (b) a uranium ADS target.

**Table 1.** Fitted data coefficients for spallation-energy-integrated uranium reaction cross sections for lead and uranium ADS targets per Eq. 18(a); Fit formula: $\langle\sigma(r)\rangle = \langle\sigma(\boldsymbol{r_0})\rangle\left[\alpha e^{-r/r_a} + (1-\alpha)e^{-r/r_b}\right]$.

| Isotope/Reaction/ADS Target | $r < 100$ cm | | | | $100 < r < 500$ cm | | | | $r > 500$ cm | | | |
|---|---|---|---|---|---|---|---|---|---|---|---|---|
| | $\sigma(0)$ (barns) | $\alpha$ | $r_a$ (cm) | $r_b$ (cm) | $\sigma(100)$ (barns) | $\alpha$ | $r_a$ (cm) | $r_b$ (cm) | $\sigma(500)$ (barns) | $\alpha$ | $r_a$ (cm) | $r_b$ (cm) |
| **U-238/Absorption/Pb** | 0.4119 | 0.6094 | 11.75 | 66.31 | 0.0372 | 0.4529 | 48.73 | 245.3 | 0.00411 | 0.7161 | 232.0 | 1050 |
| **U-238/Absorption/U** | 0.1914 | 0.3682 | 13.87 | 102.9 | 0.0465 | 0.4004 | 69.10 | 252.1 | 0.00588 | 0.7325 | 230.8 | 1132 |
| **U-238/ng/Pb** | 0.0608 | 0.2204 | 48.85 | 321.3 | 0.3646 | 0.3889 | 127.4 | 834.6 | 0.01446 | 0.4500 | 392.0 | 8062 |
| **U-238/ng/U** | 0.1200 | 0.1729 | 50.98 | 280.8 | 0.0725 | 0.4456 | 125.8 | 1086 | 0.02922 | 0.3719 | 387.3 | 10740 |
| **U-238/fission/Pb** | 0.3336 | 0.5357 | 13.21 | 63.48 | 0.0334 | 0.5605 | 50.78 | 381.1 | 0.00530 | 0.5370 | 323.5 | 2436 |
| **U-238/fission/U** | 0.1097 | 0.4386 | 15.21 | 68.78 | 0.0149 | 0.5388 | 51.36 | 351.0 | 0.00226 | 0.6258 | 326.2 | 1989 |
| **U-239/Absorption/Pb** | 0.4332 | 0.5481 | 12.84 | 134.8 | 0.0953 | 0.3353 | 78.87 | 631.2 | 0.03414 | 0.4659 | 401.9 | 7490 |
| **U-239/Absorption/U** | 0.3460 | 0.2152 | 16.02 | 192.8 | 0.1628 | 0.4245 | 108.7 | 1003 | 0.06488 | 0.3593 | 399.1 | 12080 |
| **Np-239/Absorption/Pb** | 0.3488 | 0.5328 | 12.07 | 122.1 | 0.0738 | 0.3479 | 77.31 | 470.0 | 0.02089 | 0.6109 | 382.5 | 2394 |
| **Np-239/Absorption/U** | 0.3385 | 0.1902 | 9.302 | 168.4 | 0.1536 | 0.4770 | 112.1 | 969.4 | 0.05541 | 0.3887 | 390.9 | 12110 |
| **Pu-239/Absorption/Pb** | 1.6911 | 0.3181 | 17.97 | 179.8 | 0.6687 | 0.3254 | 91.18 | 661.5 | 0.25113 | 0.4654 | 395.4 | 7789 |
| **Pu-239/Absorption/U** | 1.7588 | 0.1603 | 26.27 | 246.3 | 0.9923 | 0.3935 | 120.9 | 958.2 | 0.41209 | 0.3878 | 392.5 | 10230 |

**Table 2.** Fitted data coefficients for spallation-energy-integrated thorium reaction cross sections for lead and uranium ADS targets per Eq. 34; Fit formula: $\langle\sigma(r)\rangle = \langle\sigma(\boldsymbol{r_0})\rangle\left[\alpha e^{-r/r_a} + (1-\alpha)e^{-r/r_b}\right]$.

| Isotope/Reaction/ADS Target | $r < 100$ cm | | | | $100 < r < 500$ cm | | | | $r > 500$ cm | | | |
|---|---|---|---|---|---|---|---|---|---|---|---|---|
| | $\sigma(0)$ (barns) | $\alpha$ | $r_a$ (cm) | $r_b$ (cm) | $\sigma(100)$ (barns) | $\alpha$ | $r_a$ (cm) | $r_b$ (cm) | $\sigma(500)$ (barns) | $\alpha$ | $r_a$ (cm) | $r_b$ (cm) |
| **Th-232/Absorption/Pb** | 0.4025 | 0.6660 | 16.00 | 149.0 | 0.0698 | 0.1389 | 57.77 | 244.5 | 0.01187 | 0.8509 | 235.6 | 1133 |
| **Th-232/Absorption/U** | 0.1995 | 0.2866 | 16.66 | 173.2 | 0.0802 | 0.3292 | 104.0 | 288.4 | 0.01408 | 0.7890 | 241.6 | 1073 |
| **Th-232/ng/Pb** | 0.0895 | 0.1178 | 70.75 | 310.1 | 0.0598 | 0.5355 | 177.9 | 723.4 | 0.01938 | 0.5855 | 320.6 | 3873 |
| **Th-232/ng/U** | 0.1581 | 0.2640 | 85.68 | 339.4 | 0.0317 | 0.4373 | 140.3 | 611.4 | 0.03173 | 0.5872 | 343.3 | 3186 |
| **Th-232/fission/Pb** | 0.1332 | 0.5786 | 18.86 | 142.3 | 0.0997 | 0.1934 | 59.92 | 252.4 | 0.00480 | 0.7609 | 229.5 | 1622 |
| **Th-232/fission/U** | 0.0337 | 0.3934 | 18.18 | 172.8 | 0.0072 | 0.2173 | 91.44 | 255.3 | 0.00194 | 0.7882 | 222.8 | 1513 |
| **Th-233/Absorption/Pb** | 0.2806 | 0.5572 | 16.44 | 213.4 | 0.0962 | 0.3494 | 111.4 | 528.1 | 0.02479 | 0.5417 | 322.6 | 4250 |
| **Th-233/Absorption/U** | 0.2060 | 0.1936 | 13.14 | 218.7 | 0.1058 | 0.4023 | 132.9 | 616.9 | 0.03526 | 0.5654 | 353.9 | 3207 |
| **Pa-233/Absorption/Pb** | 0.6868 | 0.4615 | 17.29 | 215.9 | 0.2344 | 0.3506 | 116.2 | 532.2 | 0.07486 | 0.5446 | 318.7 | 4715 |
| **Pa-233/Absorption/U** | 0.8230 | 0.1177 | 19.72 | 209.3 | 0.4519 | 0.4558 | 125.9 | 604.2 | 0.13580 | 0.5778 | 348.0 | 3481 |
| **U-233/Absorption/Pb** | 0.6971 | 0.1492 | 17.87 | 255.6 | 0.4019 | 0.4620 | 162.0 | 595.1 | 0.12638 | 0.6137 | 323.2 | 2975 |
| **U-233/Absorption/U** | 0.9998 | 0.0801 | 33.25 | 265.0 | 0.6349 | 0.4188 | 143.7 | 650.1 | 0.21625 | 0.5759 | 360.8 | 3056 |

The reactions for Pu-239 production via the channel of Eq. (12) form a linear system of 1st-order Ordinary Differential Equations (ODEs). Although we assume the U-238 density is essentially constant, we can show consistency with a basic calculation of the transmutation rate for U-238:

$$\dot{n}_{\text{U-238}}(r,t) = -n_{\text{U-238}}(r,t)R^{(\text{abs})}_{\text{U-238}}(r) \tag{19}$$

where $n$ is the number density ($\text{cm}^{-3}$) of the isotope, and which is easily solved as

$$n_{\text{U-238}}(r,t) = n_{\text{U-238}}(r,0)\exp\left[-R^{(\text{abs})}_{\text{U-238}}(r)\cdot t\right] \tag{20}$$

The terms $E_p$, $d$ and $L$ have not been included for clarity, but are variable input parameters per Eqs. (13) to (16).

The fastest rate of transmutation would occur at $r = 0$, and for a typical ADS accelerator of 1 GeV/1 mA average power, and a uranium ADS cylindrical target of dimensions 20x60 cm, the reaction rate $R^{(\text{abs})}_{\text{U-238}}(r=0) = 1.3\text{x}10^{-11}$ $\text{sec}^{-1}$, or an equivalent half-life of 1,700 years. Thus, even after 5 years of continuous irradiation by such an ADS system, the uranium blanket would still have over 99% of its original U-238 density available. Our assumption of a constant U-238 density therefore is appropriate.

Starting with the first ODE for U-239 production through neutron capture by U-238:

$$\dot{n}_{\text{U-239}}(r,t) = R^{(\text{n}\gamma)}_{\text{U-238}}(r)n_{\text{U-238}} - n_{\text{U-239}}(r,t)\left(R^{(\text{abs})}_{\text{U-239}}(r) + \ln 2/\tau^{(1/2)}_{\text{U-239}}\right) \tag{21}$$

where the first term creates U-239 and the subsequent terms transmute U-239, and $\tau$ is the half-life of the isotope. The solution to this ODE is

$$n_{\text{U-239}}(r,t) = n_{\text{U-238}}\frac{R^{(\text{n}\gamma)}_{\text{U-238}}(r)}{R^{(\text{abs})}_{\text{U-239}}(r)+\ln 2/\tau^{(1/2)}_{\text{U-239}}}\left\{1-\exp\left[-(R^{(\text{abs})}_{\text{U-239}}(r)+\ln 2/\tau^{(1/2)}_{\text{U-239}})t\right]\right\} \tag{22}$$

Thus, it can be seen that the steady-state amount of U-239 produced is just the U-238 density scaled by the ratio of U-239 creation and decay rates. Similarly, the ODE for Np-239 production from U-239 is

$$\dot{n}_{\text{Np-239}}(r,t) = n_{\text{U-239}}(r,t)\ln 2/\tau^{(1/2)}_{\text{U-239}} - n_{\text{Np-239}}(r,t)\left(R^{(\text{abs})}_{\text{Np-239}}(r) + \ln 2/\tau^{(1/2)}_{\text{Np-239}}\right) \tag{23}$$

This ODE can also be solved analytically, but since Eq. (23) includes the time-dependent $n_{\text{U-239}}(r,t)$ term of Eq. (22), the solution is too long for depiction here. However, the steady state solution for $n_{\text{Np239}}(r)$ is easily solved as

$$n_{\text{Np-239}}(r) = n_{\text{U-239}}(r)\frac{\ln 2/\tau^{(1/2)}_{\text{U-239}}}{R^{(\text{abs})}_{\text{Np-239}}(r)+\ln 2/\tau^{(1/2)}_{\text{Np-239}}} \tag{24}$$

where once again the steady-state Np-239 density is the U-239 steady-state density scaled by the ratio of Np-239 creation and decay rates. For Pu-239 production, the ODE is

$$\dot{n}_{\text{Pu-239}}(r,t) = n_{\text{Np-239}}(r,t)\ln 2/\tau^{(1/2)}_{\text{Np-239}} - R^{(\text{abs})}_{\text{Pu-239}}(r)\cdot n_{\text{Pu-239}}(r,t) \tag{25}$$

Here, the Pu-239 half-life is long ($2.41\text{x}10^4$ years) such that it is not included in Eq. (25), and the steady-state solution is easily seen to be

$$n_{\text{Pu-239}}(r) = n_{\text{Np-239}}(r)\frac{\ln 2/\tau_{\text{Np-239}}^{(1/2)}}{R_{\text{Pu-239}}^{(\text{abs})}(r)} \tag{26}$$

The steady-state densities as a function of radius $r$ from the ADS target surface into the uranium blanket are shown in Fig. 13 (a) and (b) for Pb and U targets, respectively. Note that the Pu-239 density is essentially constant throughout the radial dimension of the blanket, but caution should be observed here. These steady-state solutions are for infinite time passage, which is not realistic or practical since then significant quantities of unwanted isotopes will also be produced, and at large radius the denominator of Eq. (26) becomes very small and based on fits (see Fig. 12) such that there is some level of numerical effect keeping the Pu-239 density up at large radii.

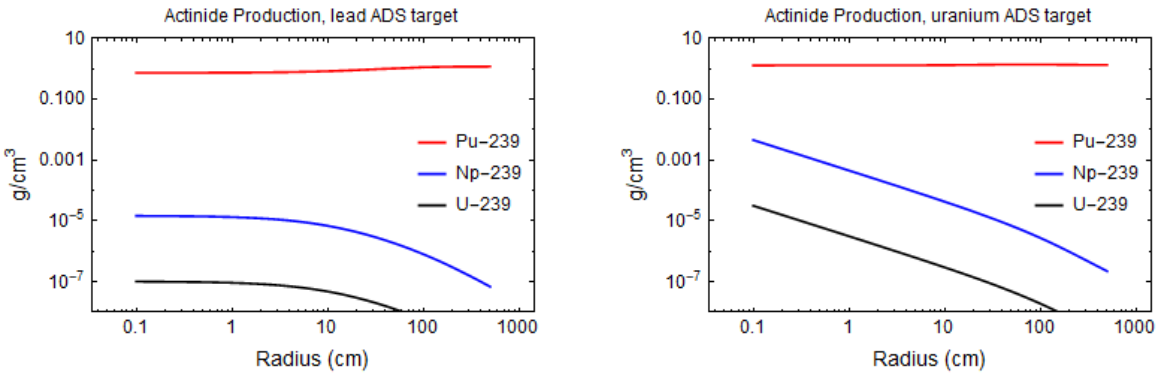


**Figure 13.** Radial distribution of steady-state actinide densities for (a) Pb ADS targets; and (b) uranium ADS targets.

## Secondary neutron flux from fission

As described by Eqs. (10) and (11), the fission of a U-238 atom releases on average 2.54 neutrons with spectrum $f_{\text{U}}^{\text{fission}}(E_n)$ at a rate of $R_{\text{U-238}}^{(\text{nf})}(E_p, r', d, L) = \phi_0^{(s)}(E_p, r', d, L) \cdot \langle\sigma_{\text{U-238}}^{(\text{nf})}(r')\rangle$, where $r'$ is used to indicate the radial location at which the fission occurred. Now, the energy-integrated, flux-decaying neutron capture cross section must be calculated for this fission spectrum and a different flux. The flux of fission neutrons can be considered equal in the forward and backward directions, given by

$$\Phi^{(f)}(E_n, E_p, r, r', d, L) = \phi_0^{(f)}(E_p, r, d, L) f^{(f)}(E_n) e^{-n_{\text{U-238}}\sigma_{\text{U-238}}^{(\text{abs})}(E_n)|r-r'|} \tag{27}$$

which is analogous to Eq. (16) and where $\phi_0^{(f)}(E_p, r, d, L) = 2.54/4\pi L(d/2 + r)$ and the superscript ($f$) indicates fission neutron flux (an additional factor of 2 is in the denominator to account for half the flux going forward and half going backward radially). Similar to Eqs. (18), the energy-dependent terms for the radiative neutron capture rate resulting from these fission neutrons can be separated and integrated over neutron energy as

$$\langle\sigma_{\text{U-238}}^{(\text{n}\gamma)}(r, r')\rangle^{(f)} = \int dE_n \cdot f^{(f)}(E_n) \exp\left[-n_{\text{U-238}}\sigma_{\text{U-238}}^{(\text{abs})}(E_n)|r - r'|\right] \cdot \sigma_{\text{U-238}}^{(\text{n}\gamma)}(E_n) \tag{28a}$$

such that

$$R_{\text{U-238}}^{(\text{n}\gamma)}\left(E_p, r, r', d, L\right)^{(f)} = \phi_0^{(f)}\left(E_p, r, d, L\right) \cdot \langle \sigma_{\text{U-238}}^{(\text{n}\gamma)}(r, r') \rangle^{(f)} \, R_{\text{U-238}}^{(\text{nf})}\left(E_p, r', d, L\right)^{(s)} \qquad (28b)$$

Note that the fission superscript denotes that the reaction is due to the secondary fission neutrons, and note that both the fission radial location $r'$ and variable radial position $r$ are included. Equation 28(b) should be convolved to account for fissions occurring anywhere from $r' = 0$ to $r_{\text{max}}$, where $r_{\text{max}}$ is the outer edge of the uranium blanket:

$$R_{\text{U-238}}^{(\text{n}\gamma)}\left(E_p, r, r_{\text{max}}, d, L\right)^{(f)} = \phi_0^{(f)}\left(E_p, r, d, L\right) \int_0^{r_{\text{max}}} \langle \sigma_{\text{U-238}}^{(\text{n}\gamma)}(r, r') \rangle^{(f)} \cdot R_{\text{U-238}}^{(\text{nf})}\left(E_p, r', d, L\right) dr' \qquad (29)$$

This fission-induced reaction rate is calculated for $r_{\text{max}}$ = 500 cm and a 20x60 cm ADS target size, as shown in Fig. 14. As shown in Fig. 14, the contribution of secondary fission neutrons to the production rate of U-239 due to the primary spallation neutrons is negligible. Therefore, enhanced production of Pu-239 from secondary fission neutrons can be ignored in Eq. (21), and all creation of U-239 is hereafter assumed to be due only to the primary spallation neutrons.

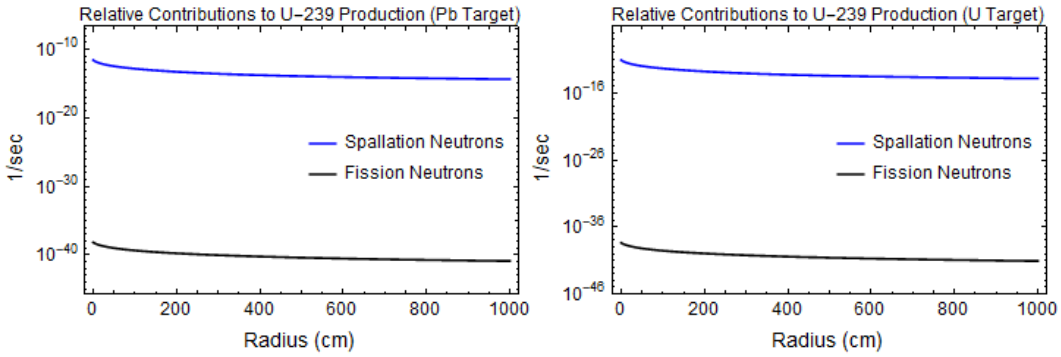


(a) (b)

**Figure 14.** Reaction rates for the creation of U-239 from U-238 for both primary spallation neutrons in comparison with secondary fission neutrons for (a) lead ADS target (20x60 cm); and (b) uranium ADS target with $r_{\text{max}}$ = 500 cm.

## Plutonium Production Results

The coupled first-order ODEs represented by Eqs. (21), (23) and (25) can each be solved analytically by first integrating Eq. (21) for U-239 production, as shown in Eq. (22), and then inserting this time-dependent solution for $n_{\text{U-239}}$ into Eq. (23) for $n_{\text{Np-239}}(t)$, and then finally inserting $n_{\text{Np-239}}(t)$ into Eq. (25) to solve analytically for $n_{\text{Pu-239}}(t)$. Alternatively, one could use standard numerical techniques to simultaneously solve all three ODEs as a system of coupled ODEs. We used Mathematica software to analytically solve each equation separately for the actinide densities as a function of time, which are not reproduced here due to the very long and complicated nature of these analytic solutions.

Our analytic solutions for Pu production should be compared to other data for confidence that our formulation is applicable. Shown in Fig. 15(a) is a comparison of our formulation against the Monte Carlo results of Englert *et al*. [26]. Englert *et al* assumed a point source of spallation neutrons in a quasi-infinite sphere of natural uranium ($r_{max}$ = 500 cm) for a 1 mA current proton beam at a variety of energies using the high energy physics and neutron transport code MCNPX [27]. As can be seen from Fig. 15(a), our model does quite well at reproducing the results of Englert et al, where we assumed an equivalent mass of uranium in a 1666 cm radius, 60 cm long cylindrical blanket to their 500 cm radius sphere. Shown in Fig. 15(b) is a comparison of our model to that of Magill & Peerani [19] as given by Eq. (13). Note that in the original article by Magill & Peerani they assumed a sphere of 50 cm radius, but this radius would allow for leakage of spallation neutrons and therefore not truly be an "infinite" sphere. Therefore, in the presentation in Englert *et al* of Magill's model they assume a radius of 500 cm equivalent solution for Magill's sphere. Thus, in Fig. 15(b) both a 50 cm radius cylindrical blanket and a 500 cm blanket are calculated, and as shown the 500 cm radius matches the Magill model much better, consistent with Englert's assumptions.

Since the results shown in Fig. 15 appear to be consistent with the limited published data, and noting that our solution incorporates the actual cross sections from the quantitative ENDF libraries, we believe we have demonstrated the accuracy of our approach.

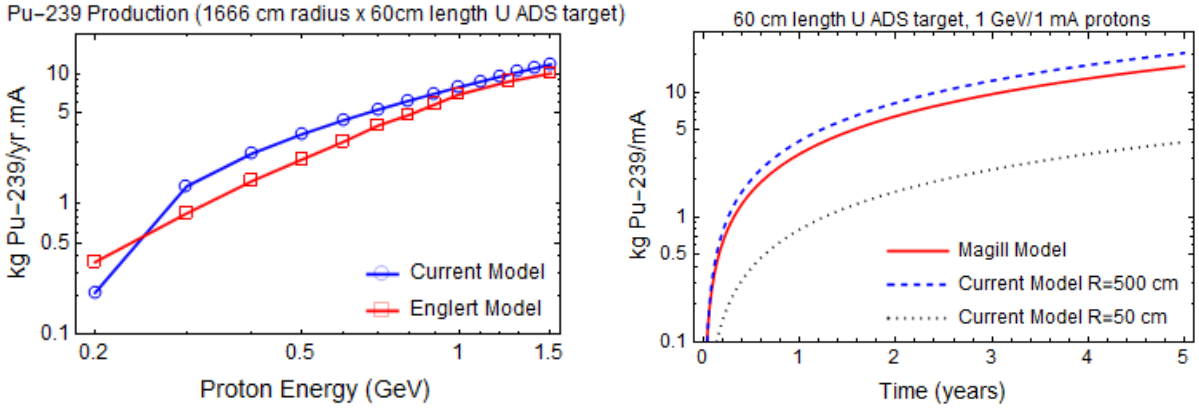


(a) (b)

**Figure 15.** Comparison of the calculation of our analytic model with the results of (a) Englert et al [26]; and (b) the simple model of Magill & Peerani [19], as given by Eq. (13).

## Thorium Fuel Cycle

A thorium blanket can replace the uranium blanket in Fig. 1 and the same procedure as described above used to calculate the production of U-233. The analogous reaction path is

$$^{232}\text{Th} \rightarrow {}^{233}\text{Th} \rightarrow {}^{233}\text{Pa} \rightarrow {}^{233}\text{U} \qquad (30)$$

where Th-233 is created through radiative neutron capture by Th-232, and Pa-233 and U-233 result from subsequent natural $\beta^-$ decays (21.83 minutes and 26.975 days, respectively).

Secondary neutrons from fission of Th-232 are neglected similarly as before since the effect is miniscule.

Production rates can be written directly from the equations developed for the uranium fuel cycle, namely,

$$\dot{n}_{\text{Th-233}}(r,t) = R^{(\text{n}\gamma)}_{\text{Th-232}}(r) n_{\text{Th-232}} - n_{\text{Th-233}}(r,t)\left(R^{(\text{abs})}_{\text{Th-233}}(r) + \ln 2/\tau^{(1/2)}_{\text{Th-233}}\right) \quad (31)$$

$$\dot{n}_{\text{Pa-233}}(r,t) = n_{\text{Th-233}}(r,t)\ln 2/\tau^{(1/2)}_{\text{Th-233}} - n_{\text{Pa-233}}(r,t)\left(R^{(\text{abs})}_{\text{Pa-233}}(r) + \ln 2/\tau^{(1/2)}_{\text{Pa-233}}\right) \quad (32)$$

$$\dot{n}_{\text{U-233}}(r,t) = n_{\text{Pa-233}}(r,t)\ln 2/\tau^{(1/2)}_{\text{Pa-233}} - R^{(\text{abs})}_{\text{U-233}}(r)\cdot n_{\text{U-233}}(r,t) \quad (33)$$

where the radially-dependent reaction rates are similarly given by

$$R^{(j)}_i(E_p,r,d,L) = \phi^{(s)}_0(E_p,r,d,L)\cdot\langle\sigma^{(j)}_i(r)\rangle \quad (34)$$

Here, $\phi^{(s)}_0$ is the same spallation neutron flux as used in Eq. (16), and the averaged radially-dependent cross sections $\langle\sigma^{(j)}_i(r)\rangle$ have been calculated again using the ENDF/B-VII.1 library. The resulting fits to this data are given in Table 2.

U-233 production can then calculated by integrating Eqs. (31) – (33) over radius, similar as was done for uranium above. Shown in Fig. 16 is the production of both Pu-239 and U-233 in natural uranium or thorium blankets, respectively, assuming a common lead ADS target (20x100 cm Pb cylinder). As shown in Fig. 16, U-233 production is slightly less than Pu-239 and both follow a similar trend with proton energy, which is expected since this trend is driven by the spallation neutron yield caused by bombarding protons.

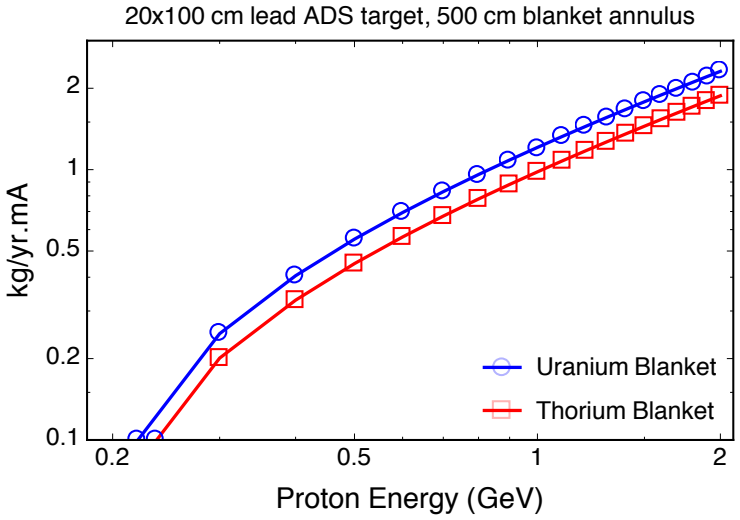


**Figure 16.** Comparison of Pu-239 and U-233 production from ADS spallation neutrons using the developed models for a 20 cm diameter, 100 cm long cylindrical lead ADS target surrounded by 500 cm annular radius of uranium or thorium fertile blankets, respectively.

## Conclusion

Published theory and experimental data for spallation neutron multiplicity was used to derive a general model of neutron yield for arbitrary ADS cylindrical target dimensions and proton energies for both uranium and lead targets. Additionally, a generalized fast spallation neutron spectrum was provided for either uranium or lead ADS targets, expanding on the nominal spectrum model of Findlay [21]. Using this improved model spectrum and the estimated spallation neutrons available entering an annular uranium or thorium blanket, and transmutation cross sections taken from the ENDF/B-VII.1 library, simplified ordinary differential equations were derived that can be easily integrated to estimate fissile material production rates. Equations were provided for both lead or uranium ADS targets and either natural uranium or thorium fertile blankets of arbitrary size. It was also shown that secondary fission neutrons are negligible in the overall fissile material production rates, so were ignored in subsequent calculations.

While this model of a cylindrical ADS Pb or U ADS target surrounded by an annular fertile blanket is a simplified picture of likely ADS implementations (see Fig. 1), since in reality the blanket would probably consist of fuel assembles and rods rather than a solid annulus, this model does seem to provide realistic fissile material production rates in comparison with other published data. The current model does not include backscattering of spallation neutrons, since it is assumed the spallation neutrons probably react just once as they traverse the blanket in the outward radial direction.

An advantage of this approach is minimizing the need to run neutronics codes, such as MCNP, for each specific ADS target and blanket design. With the current model, one can quickly estimate fissile material production rates, and then if desired run more detailed neutronics on specific designs. Further, actual cross sections were used from the ENDF/B-VII.1 library, similar to as would be used by more detailed neutronics codes, adding some confidence to the fidelity of the current model. Also, the spallation neutron yield as a function of thick ADS target dimensions and bombarding proton energy, as given by Eqs. (5) & (6), is immediately useful to decide upon optimal target parameters paired to a given accelerator.

Future work could include adding a moderator between the ADS target and blanket material. While a thermal neutron spectrum may not benefit a natural uranium target in regards to Pu-239 production, slower neutrons may enhance U-233 production from thorium blankets. Also not evaluated here was partition and transmutation (P&T) of other isotopes, which would be necessary to properly address using ADS as a spent fuel burner, or to better quantify signatures passively emanating from target material or present during active interrogation for signatures.

## Bibliography


[1] G. S. Bauer, "Physics and technology of spallation neutron sources," *Nuclear Instruments and Methods in Physics Research A,* vol. 463, pp. 505-543, 2001.

[2] D. Hilscher, U. Jahnke, F. Goldenbaum, L. Pienkowski, J. Galin and B. Lott, "Neutron production by hadron-induced spallation reactions in thin and thick Pb and U targets from1 to 5 GeV," *Nuclear Instruments & Methods in Physics Research A,* vol. 414, pp. 100-116, 1998.

[3] A. Letourneau, J. Galin, F. Goldenbaum, B. Lott, A. Peghaire, M. Enke, D. Hilscher, U. Jahnke, K. Nunighoff, D. Filges, R. D. Neef, N. Paul, H. Schaal, G. Sterzenbach and A. Tietze, "Neutron production in bombardments of thin and thick W, Hg, Pb targets by 0.4, 0.8, 1.2, 1.8, and 2.5 GeV protons," *Nuclear Instruments & Methods in Physics Research B,* vol. 170, pp. 299-322, 2000.

[4] L. Pienkowski, F. Goldenbaum, D. Hilscher, U. Jahnke, J. Galin and B. Lott, "Neutron multiplicity distributions for 1.94 to 5 GeV/c proton-, antiproton-, pion-, kaon-, and deuteron-induced spallation reactions on thin and thick targets," *Physical Review C,* vol. 56, pp. 1909-1917, 1997.

[5] S. R. Hashemi-Nezhad, W. Westmeier, M. Zamani-Valasiadou, B. Thomauske and R. Brandt, "Optimal ion beam, target type and size for accelerator driven systems: Implications to the associated accelerator power," *Annals of Nuclear Energy,* vol. 38, pp. 1144-1155, 2011.

[6] J. Cugnon, C. Volant and S. Vuiller, "Nucleon and deuteron induced spallation reactions," *Nuclear Physics A,* vol. 625, pp. 729-757, 1997.

[7] J. Cugnon, C. Volant and S. Vuillier, "Improved intranuclear cascade model for nucleon-nucleus interactions," *Nuclear Physics A,* vol. 620, pp. 475-509, 1997.

[8] J. Cugnon, "Proton-nucleus interaction at high energy," *Nuclear Physics A,* vol. 462, pp. 751-780, 1987.

[9] V. I. Yurevich, "Neutron production in pA and AA collisions at intermediate energies," *Physics of Particles and Nuclei,* vol. 40, pp. 49-66, 2009.

[10] V. I. Yurevich, R. M. Yakovlev and V. G. Lyapin, "Neutron emission in interactions of 1H, 2H, 4He, and 12C nuclei with lead nuclei at 1-2 GeV per nucleon," *Physics of atomic nuclei,* vol. 69, pp. 1496-1509, 2006.

[11] V. I. Yurevich, R. M. Yakovlev, V. A. Nikolaev, V. G. Lyapin and N. S. Amelin, "Investigation of neutron emission in the interaction of relativisitic protons and deuterons with lead targets," *Physics of Particles and Nuclei Letters,* vol. 3, pp. 169-182, 2006.

[12] C. -M. Herbach, D. Hilscher, U. Jahnke, V. G. Tishchenko, J. Galin, A. Letourneau, A. Peghaire, D. Filges, F. Goldenbaum, L. Pienkowski, W. U. Schroder and J. Toke, "Systematic investigation of 1.2 GeV proton-induced spallation reactions on targets between Al and U," *Nuclear Instruments and Methods in Physics A,* vol. 562, pp. 729-732, 2006.

[13] V. I. Yurevich, "Production of neutrons in thick targets by high-energy protons and nuclei," *Physics of Particles and Nuclei,* vol. 41, pp. 778-825, 2010.

[14] V. A. Nikolaev, V. I. Yurevich, R. M. Yakovlev and R. G. Vassil'kov, "Neutron production in thick lead target," in *ICANS-XI International Collaboration on Advanced Neutron Sources*, Tsukuba, 1990.

[15] R. G. Vassil'kov and V. I. Yurevich, "Neutron emission from an extended lead target under the action of light ions in the GeV region," in *ICANS-XI International Collaboration on Advanced Neutron Sources*, Tsukuba, 1990.

[16] J. M. Carpenter, "Pulsed spallation neutron sources for slow neutron scattering," *Nuclear Instruments & Methods,* vol. 145, pp. 91-113, 1977.

[17] M. Arai, Y. Kiyanagi, N. Watanabe, R. Takagi, H. Shibazaki, M. Numajiri, S. Itoh, T. Otomo, M. Furusaka, Y. Inamura, Y. Ogawa, Y. Suda and S. Satoh, "Neutron production from lead largets for 12-GeV protons," *Journal of Neutron Research,* vol. 8, pp. 71-83, 1999.

[18] J. S. Fraser, R. E. Green, J. W. Hilborn, J. C. D. Milton, W. A. Gibson, E. E. Gross and A. Zucker, "Neutron production in thick targets bombarded by high energy protons," *Physics in Canada,* vol. 21, pp. 17-18, 1965.

[19] J. Magill and P. Peerani, "(Non-) proliferation aspects of Accelerator Driven Systems," *Journal of Physics IV France,* vol. 9, pp. Pr7-167, 1999.

[20] J. S. Gilmore, G. J. Russell, H. Robinson and R. E. Prael, "Fertile-to-fissile and fission measurements for depleted uranium and thorium bombarded by 800-MeV protons," *Nuclear Science & Engineering,* vol. 99, pp. 41-52, 1988.

[21] D. J. Findlay, "A simple representation of spallation neutron energy spectra for 'back of the envelope' estimates," *Applied Radiation and Isotopes,* vol. 121, pp. 61-63, 2017.

[22] T. Ethvignot, M. Devlin, H. Duarte, T. Granier, R. C. Haight, B. Morillon, R. O. Nelson, J. M. O'Donnel and D. Rochman, "Neutron multiplicity in the fission of 238U and 235U with neutrons up to 200 MeV," *Physical Review Letters,* vol. 94, p. 052701, 2005.

[23] R. B. Leachman, "Emission of prompt neutrons from fission," *Physical Review,* vol. 101, pp. 1005-1011, 1956.

[24] L. M. Petrie, W. C. Jordon, A. L. Edwards, P. T. Williams, J. C. Ryman, O. W. Hermann, N. F. Landers, J. A. Bucholz, J. R. Knight, C. V. Parks, J. C. Turner, R. M. Westfall, J. T. West, M. B. Emmett and N. M. Greene, "SCALE: A modular code system for performing standardized computer analyses for licensing evaluation," ORNL, Oak Ridge, 1995.

[25] F. T. Binford, "Diversion assumptions for high-powered research reactors," ORNL, Oak Ridge, 1984.

[26] M. Englert, C. Pistner and W. Liebert, "Neutronics calculations for the assessment of proliferation risks associated with spallation neutron sources," *Nuclear Instruments and Methods in Physics Research A,* vol. 562, pp. 557-560, 2006.

[27] L. S. Waters, "MCNPX User's Manual," LANL, 2002.

[28] M. Fragopoulou, M. Manolopoulou, S. Stoulos, R. Brandt, W. Westmeier, B. A. Kulakov, M. I. Krivopustov, A. N. Sosnin, M. Debeauvais, J. C. Adloff and M. Zamani-Valasiadou, "Spatial distribution of moderated neutrons along a Pb target irradiated by high-energy protons," *Nuclear Instruments & Methods in Physics Research A,* vol. 560, pp. 571-576, 2006.